

## **Underestimation of deep convective cloud tops by thermal imagery**

Steven C. Sherwood, Jung-Hyo Chae

Department of Geology and Geophysics, Yale University, New Haven, CT, USA

Patrick Minnis

NASA/Langley Research Center, Hampton, Virginia

Matthew McGill

NASA/Goddard Space Flight Center, Greenbelt, Maryland

Short title: CLOUD TOP HEIGHTS

**Abstract.** The most common method of ascertaining cloud heights from space is from thermal brightness temperatures. Deep cumulus clouds of high water content are expected to radiate as black bodies. Here, cloud tops are estimated from several sensors: GOES-8, the Moderate Resolution Imaging Spectroradiometer (MODIS), the Moderate resolution Imaging Sensor (MISR), and the Goddard Cloud Physics Lidar (CPL), all collected during the CRYSTAL Florida Area Cirrus Experiment (CRYSTAL-FACE). Thermally derived cloud tops are consistently  $\sim 1$ km too low compared with independent measurements, no matter how thick the clouds are, even when the finite optical extinctions near cloud top and in thin overlying cirrus are taken into account. The bias appears to get worse for the tallest clouds. Cloud material is often present 2 km or more above the apparent cloud top. This mysterious discrepancy appears to be satellite-independent.

## Introduction

Since the first weather satellites in the 1960's, thermal imagery has been an invaluable source of information on cloud heights and storm severity. One can locate the approximate top of an opaque cloud by observing its effective blackbody temperature ("brightness temperature"  $T_\lambda$ ) at some wavelength  $\lambda$  that passes easily through air (e.g.,  $\sim 10\text{-}12\ \mu\text{m}$ ), and matching this to a local atmospheric sounding [Smith and Platt, 1978] to obtain a height  $Z_\lambda$ . This continues to be a mainstay of cloud-related research, due to the wide availability of infrared data and simplicity of the method. An important complication is that in many cases, emission from below cloud top transmits either through the cloud itself or through gaps, inflating  $T_\lambda$  relative to the true cloud-top temperature. Photon scattering can also enter the problem. Much work has been done on addressing these issues for thin or broken clouds using multiple wavelengths [e.g. Minnis *et al.*, 1998; Platnick *et al.*, 2003; Smith and Platt, 1978].

These complications are not thought to be significant for deep convective clouds, due to their high water contents. Other errors may arise, due to cloud heterogeneity and cloud-environment temperature differences, but corrections would require detailed information on the cloud, so it is typically just treated as a black body at the environmental temperature. There are indications from case studies [e.g. Smith, 1992] that this may underestimate cloud heights.

The importance of knowing deep cumulus heights accurately is underscored by some recent developments. For example, intense updrafts are responsible for the creation of hailstones and lightning [Zipser and Lutz, 1994]. A wealth of recent data has illustrated how strongly lightning prefers continents, but we still do not know why [Williams and Stanfill, 2002]. Cumulus mixing effects near the tropopause, which may be important for tracer transport and energy budgets [Alcala and Dessler, 2002; Fromm and Servranckx, 2003; Gettelman *et al.*, 2002; Sherwood *et al.*, 2003], are also sensitive to small changes in penetration depth. Here we examine thermal cloud top estimates using data from soundings and several remote-sensing instruments associated with the CRYSTAL Florida Area Cirrus Experiment (CRYSTAL-FACE) during July 2002 [Jensen *et al.*, 2003].

## Computation of thermal Cb heights

We obtained 4-km infrared ( $10.8 \mu\text{m}$ ) brightness temperatures  $T_{11}$  taken every 15 minutes by the eighth Geostationary Operational Environmental Satellite (GOES-8). Calibration of the GOES-8 infrared radiances is maintained using on-board blackbodies. The GOES-8 data have also been compared with radiances from similar channels on two research satellites [Minnis *et al.*, 2002] and agree to within  $\pm 0.5$  K over the full range of temperatures, on average. Cloud temperatures were derived together with other cloud parameters using radiative transfer model parameterizations that account for ice cloud scattering and emission [Minnis *et al.*, 1995, 1998]. For deep convective clouds of specific interest here, these derived temperatures do not differ significantly from  $T_{11}$ .

Cloud heights  $Z_{11}$  were determined by two methods. The first, available from the NASA Langley group as a GOES CRYSTAL product (see [angler.larc.nasa.gov/crystal/](http://angler.larc.nasa.gov/crystal/)), uses hourly temperature profiles provided by the Rapid Update Cycle 20-km analyses [Benjamin *et al.*, 2004] by finding the lowest altitude having the estimated GOES-8 cloud temperatures. The second uses several candidate cloud-temperature ( $T(Z)$ ) models based on local radiosonde data to convert  $T_{11}$  directly to height. Heights from the two methods do not differ by more than  $\sim 100$  meters, except for the very tallest clouds where the result begins to depend on the  $T(Z)$  model. We present only  $Z_{11}$  results from the second procedure. 11 and 12-micron results were similar for optically thick clouds.

Radiosondes were obtained from Key West, Miami, and the CRYSTAL-FACE Western Ground site (81.4W, 25.8N). A “reference sounding” was obtained for each pixel by the following procedure. Pixels near Key West (within about 100 km) were assigned the Key West sounding taken at the nearest available observing time. Those over the peninsula were assigned the mean of the soundings from Miami, the Western Ground site, and Tampa at the nearest available observing time. Other ocean pixels were assigned the mean of all four stations. In general the temperatures did not differ much among the stations, so it is unlikely that significant errors arise from temperature variability on meso- or synoptic scales. The “nearest available observing time” is taken to be the closest time of day at which there is a

least one observation available from the station(s) in question. Finally, the temperature profiles were smoothed slightly in the vertical using a moving weighted window of width 15 hPa, to reduce features comparable to or smaller than a photon mean free path.

### **Cloud temperature assumption**

A height  $Z_{11}$  was computed for each GOES-8 pixel using the appropriate reference profile, by simply assigning the lowest pressure and altitude where the profile matches the 11 micron brightness temperature  $T_{11}$ . This implies an assumption that the cloud temperature will be the same as that of a distant environment at the same altitude. Through most of the troposphere, the interior of thermals tends to be several K warmer than the environment, but this anomaly decreases toward cloud top due to adiabatic cooling and mixing. For overshooting convective clouds, however, adiabatic cooling dominates and the cloud temperature can be cooler than the environment, by as much as 20 K in the most extreme cases [e.g. *Adler and Mack*, 1986]. Occasionally, though rarely over Florida,  $T_{11}$  is below any temperature in the sounding.

Not knowing exactly how to correct for this, we tried three candidate procedures. The first, or “adiabatic-1” involves replacing temperatures above the WMO (lapse-rate) tropopause with an adiabat intersecting the observed profile at the tropopause level. “Adiabatic-2” follows the same procedure except starting 40 hPa below the WMO tropopause. The reason for this is that clouds are probably already colder than their environment by the time they reach the tropopause; 40 hPa is found to be far enough below this so that the the lapse rate is fairly close to an adiabat and cloud buoyancies are likely to be near neutral. Finally, we consider a “semiadiabatic” profile which is just the average of the adiabatic-2 and environmental ones, representing the likely result of a cloud actively mixing with its environment.

## **Evaluation**

### **Thermal vs. CPL lidar**

The CRYSTAL-FACE mission included the Cloud Physics Lidar (CPL), which flew on board the NASA ER-2 high-altitude research aircraft. The CPL is a multi-wavelength elastic

backscatter lidar that provides cloud and aerosol profiling with 30 m vertical and 1 second temporal resolution. Details of CPL data analysis can be found in *McGill et al.* [2003]. Important features of the CPL design are a small receiver field of view (100 microradians full angle) to minimize multiple scattering, and high sensitivity detectors, revealing thin cloud and aerosol layers that are undetectable by other sensors. The frequent imaging by GOES-8 allows each CPL observation to be co-located to a neighboring satellite pixel taken within eight minutes. For this comparison, the impact of the  $T(Z)$  models were insignificant.

The estimate  $Z_{11}$  represents a “radiometric” cloud top. This should occur one photon penetration depth into the cloud if the Planck function  $B(\tau)$  is linear in optical depth  $\tau$  and there is no scattering, as can be seen by substituting such a linear relationship into the solution

$$I_{\text{TOA}} = \int_0^{\infty} B(\tau)e^{-\tau} d\tau \quad (1)$$

of Schwarzschild’s equation, which yields  $I_{\text{TOA}} = B(1)$ , or  $T_{11} = T(1)$ . Numerical evaluation of (1) with reasonable nonlinearities in  $B(\tau)$  expected for cloud top regions yields  $T_{11}$  up to 2 K colder than  $T(1)$ . Inclusion of scattering may reasonably lead to  $T_{11} = T(2)-T(3)$  or so, if scattering goes primarily into a forward peak and the single-scatter albedo is in the range 0.5 – 0.7. Thus, we should compare  $Z_{11}$  with heights determined by the lidar to lie at cloud optical depths of 1-3. This is readily done by integrating the volumetric extinctions provided by the CPL downward from the top of the first aerosol or cloud layer detected, until selected  $\tau$  values are attained; the resulting heights will be denoted  $Z_{\text{lid}}(1)$ ,  $Z_{\text{lid}}(2)$ , etc.

Figure 1 compares  $Z_{\text{lid}}(1)$  with  $Z_{11}$  from GOES-8. Each point represents a lidar dwell, colocated to the nearest GOES pixel. Points far off the diagonal are due to optically thin clouds ( $Z_{11} < Z_{\text{lid}}(1)$ ) or points just beyond cloud edges ( $Z_{11} > Z_{\text{lid}}(1)$ ). The central cluster of points comes from thick, beam-filling clouds. In this group a roughly 1-km bias is clearly evident, with  $Z_{11}$  too low. The scatter in this group is no greater than 1 km, so this bias is a broad influence on most pixels rather than an episodic error. Comparisons with  $Z_{\text{lid}}(2)$  and  $Z_{\text{lid}}(3)$  are similar, since these depths lie typically only about 100 and 150 m, respectively, below  $Z_{\text{lid}}(1)$ . Although the lidar loses sensitivity below optical depths of 3-4, reasonable extrapolations of optical depth using qualitative information from the two radars on board the

ER-2 suggest that  $Z_{11}$  appears to lie near  $\tau \sim 20$  or more.

One often assumes that clouds will have a sharp upper boundary, but glaciated clouds typically have fuzzy edges even in regions of active convection. Further, thin laminar clouds may form above the main cumulus cell. Figure 2 shows composite retrievals of volumetric extinction coefficient (a proxy for cloud ice concentration if variations in particle size and shape are neglected) as a function of the distance above  $Z_{\text{lid}}(1)$ , above clouds over the peninsula. The lidar shows that cloud material extending above this level decreases in a quasi-exponential manner, with a characteristic vertical scale of a few hundred meters. Combining this with the 1 km bias, we find that cloud material may be found up to 2 km above the GOES-estimated, thermal “cloud top.”

### **Thermal vs. MISR**

Due to the puzzling height discrepancy, we felt it worthwhile to investigate further using two platforms on board NASA’s Terra satellite, MODIS and MISR. There were three Terra overpasses during the experiment (July 9, 18, and 20) that contained sufficient quantities of deep convective cloud.

We used MODIS Channel 31 (11.03  $\mu\text{m}$ ) to obtain  $Z_{11}$ . *Minnis et al.* [2002] found biases between MODIS and GOES-8 to be less than 0.5 K, equivalent to less than 100 m altitude. The similarity of  $T_{11}$  and  $T_{12}$  in the GOES-8 data argues that the choice of wavelength is not critical either. We followed the same procedure to convert brightness temperature to  $Z_{11}$  as for GOES-8, except that the Miami sounding was used for all pixels. The product we used was the MODIS level 1B calibrated, geolocated radiances (MOD02)[*King et al.*, 2003].

We compared MODIS  $Z_{11}$  with the stereoscopic heights  $Z_{\text{ster}}$  from the MISR “best winds,” top-of-atmosphere (TOA)/cloud product, Version 8. The stereoscopic method involves viewing the same cloud from several different angles to determine its height from its apparent displacements relative to the surface. The “best winds” product exploits orbital and surface curvature to estimate cloud-top horizontal motion and height simultaneously [*Moroney et al.*, 2002]. Their “no-winds” product appeared to correlate more poorly with radiometric heights.

We used the stereoscopically-derived cloud mask and the stereoscopic override flag to remove pixels that were clear or near the surface, and any pixels with override problems.

A limb parallax correction was required for proper horizontal collocation of the two instruments, since the MISR retrievals are georegistered to the ground directly below the cloud, while the MODIS data are georegistered to the ground location that would have been in view under clear-sky conditions. The terrain height, cloud height, and angle of view information necessary for this correction were obtained from the MOD03 product. The correction had only a small effect on the comparison, due to typically large cloud shields (no parallax correction was deemed necessary for the GOES-lidar comparisons owing to the coarser resolution and high zenith angle of GOES-8).

The height results, compared in Figure 3, confirm the difference noted earlier. Furthermore, since the data now extend to somewhat higher cloud tops, we can investigate their behavior more carefully. We do this by computing histograms, shown in Figure 4, of  $Z_{11}$  from each the different  $T(Z)$  models, and  $Z_{\text{ster}}$  from MISR. We see that, while the choice of  $T(Z)$  model has some an impact on the comparison, this is much less than the difference between instruments. Further, while  $Z_{11}$  appears to saturate near  $\sim 14$  km,  $Z_{\text{ster}}$  possesses a tail of very high values reaching almost 2 km above the highest thermal ones even using the most favorable (adiabatic-2)  $T(Z)$  relation. This tail could be a noise artifact, but otherwise it suggests that the low bias in thermal height estimates may actually get worse for the tallest clouds.

Efforts to identify cloud properties that are related to the bias have met with limited success. The cold-cloud bias is about 100 m smaller in  $Z_{12}$  than  $Z_{11}$ , and mitigates slightly with increasing cloud albedo.

## Discussion

The 5-7 K, 1-km bias between visible and infrared top heights is puzzlingly large, easily standing out above the variability among beam-filling, opaque clouds. It evidently cannot be due to satellite or radiosonde calibration problems, since instrument comparisons

limit uncertainties in both to an order of magnitude less than needed. We can only list and discuss several other possible sources of error, in no particular order: i) Within-pixel cloud heterogeneity or “beam-filling” errors; ii) finite cloud emissivity; iii) IR scattering and/or differences in visible extinction and IR absorption cross sections; iv) nonlinear emission profile  $B(\tau)$ ; v) cloud-environment temperature differences; vi) stray light in the infrared optics.

Unfortunately, none of these explanations seems satisfactory on its own. Cloud heterogeneity can cause biases due to the nonlinearity of  $B(T)$ , but tests with MODIS data indicate that heterogeneity on the 1-km scale contributes less than 1 K of warm bias, and achieving large biases requires that pixels have a mixture of clear sky and thick deep cloud, an occurrence far too rare to explain the results. Models indicate that for cloud temperatures below about 230 K, scattering should not significantly affect  $T_{11}$  [Minnis *et al.*, 1998], at least for plane-parallel clouds. The nonlinearity of  $B(\tau)$  and cloud-environment temperature differences each produce errors that should make clouds appear too high rather than too low.

Cloud optical depths will be greater in visible than infrared wavelengths if many small particles are present. To account for the entire bias, however, one would need most of the total particle surface area in the upper part of the cloud to be in particle diameters much less than  $10\mu\text{m}$ , whereas in-situ observations indicate median-area diameters somewhat greater than  $10\mu\text{m}$  [Garrett *et al.*, 2003].

Stray light or crosstalk from warmer parts of the scene could scatter into the cold pixels, biasing all observations toward the field-of-view mean. Most on-board calibration and many intercomparison procedures would not detect such a problem, but the consistency of the bias between at least two different satellites argues against this explanation in favor of one rooted in cloudy radiative transfer.

In summary, the thermal warm bias remains a mystery. Though small compared to the dynamic range of observed cloud heights, this difference is nonetheless significant from the perspective of differentiating intense storms or quantifying troposphere-stratosphere mixing. We hope that continued research will yield explanations.

**Acknowledgments.** We thank Roger Davies for assistance and advice regarding MISR data,

Heidi Zeleznik for data management, Chris Moeller and Tim Garrett for useful discussions, and Dennis Hlavka for assistance with CPL data. This work was supported by NASA EOS/IDS grant NAG-59632 and NAG5-12056.

## References

- Adler, R. F., and R. A. Mack, Thunderstorm cloud top dynamics as inferred from satellite observations and a cloud top parcel model, *J. Atmos. Sci.*, *43*, 1945–1960, 1986.
- Alcala, C. M., and A. E. Dessler, Observations of deep convection in the Tropics using the Tropical Rainfall Measuring Mission TRMM precipitation radar, *J. Geophys. Res.*, *107*, art. no.–4792, 2002.
- Benjamin, S. G., et al., An hourly assimilation/forecast cycle: The Ruc., *Mon. Weather Rev.*, p. In Press, 2004.
- Fromm, M. D., and R. Servranckx, Transport of forest fire smoke above the tropopause by supercell convection, *Geophys. Res. Lett.*, *30*, 10.1029/2002GL016,820, 2003.
- Garrett, T. J., H. Gerber, D. G. Baumgardner, C. H. Twohy, and E. M. Weinstock, Small, highly reflective ice crystals in low-latitude cirrus, *Geophys. Res. Lett.*, *30*, 10.1029/2003GL018,153, 2003.
- Gettelman, A., M. L. Salby, and F. Sassi, Distribution and influence of convection in the tropical tropopause region, *J. Geophys. Res.*, *107*, Art. No. 4080, 2002.
- Jensen, E., D. Anderson, H. Selkirk, D. Starr, and O. Toon, Overview of the Cirrus Regional Study of Tropical Anvils and Cirrus Layers - Florida Area Cirrus Experiment (CRYSTAL-FACE), *Bull. Amer. Meteorol. Soc.*, 2003.
- King, M. D., et al., Cloud and aerosol properties, precipitable water, and profiles of temperature and water vapor from MODIS, *IEEE Trans. Geoscience Remote Sensing*, *41*, 442–458, 2003.
- McGill, M., D. Hlavka, W. Hart, E. Welton, and J. Campbell, Airborne lidar measurements of aerosol optical properties during SAFARI-2000, *J. Geophys. Res.*, *108*, 10.1029/2002JD002,370, 2003.
- Minnis, P., D. P. Kratz, J. A. J. Coakley, M. D. King, D. Garber, P. Heck, S. Mayor, D. F. Young, and R. Arduini, *Clouds and the Earth's Radiant Energy System (CERES) Algorithm Theoretical Basis Document, Volume III: Cloud Analyses and Radiance Inversions (Subsystem 4)*, report #1376, vol. 3 Cloud Optical Property Retrieval (Subsystem 4.3), pp. 135–176, NASA, 1995, CERES Science Team, Eds.
- Minnis, P., D. P. Garber, D. F. Young, R. F. Arduini, and Y. Takano, Parameterization of reflectance

- and effective emittance for satellite remote sensing of cloud properties, *J. Atmos. Sci.*, *55*, 3313–3339, 1998.
- Minnis, P., L. Nguyen, D. R. Doelling, D. F. Young, W. F. Miller, and D. P. Kratz, Rapid calibration of operational and research meteorological satellite imagers, Part II: Comparison of infrared channels, *J. Atmos. Oceanic Tech.*, *19*, 1250–1266, 2002.
- Moroney, C., R. Davies, and J. P. Muller, Operational retrieval of cloud-top heights using MISR data, *IEEE Trans. Geoscience Remote Sensing*, *40*, 1532–1540, 2002.
- Platnick, S., M. D. King, S. A. Ackerman, W. P. Menzel, B. A. Baum, J. C. Riedi, and R. A. Frey, The modis cloud products: Algorithms and examples from Terra, *IEEE Trans. Geoscience Remote Sensing*, *41*, 459–473, 2003.
- Sherwood, S. C., T. Horinouchi, and H. A. Zeleznik, Convective impact on temperatures observed near the tropical tropopause, *J. Atmos. Sci.*, *60*, 1847–1856, 2003.
- Smith, R. B., Deuterium in North-Atlantic storm tops, *J. Atmos. Sci.*, *22*, 2041–2057, 1992.
- Smith, W. L., and C. M. R. Platt, Comparison of satellite-deduced cloud heights with indications from radiosonde and ground-based laser measurements, *J. Appl. Meteorol.*, *17*, 1796–1802, 1978.
- Williams, E., and S. Stanfil, The physical origin of the land-ocean contrast in lightning activity, *Comptes Rendus Physique*, *3*, 1277–1292, 2002.
- Zipser, E. J., and K. R. Lutz, The vertical profile of radar reflectivity of convective cells—a strong indicator of storm intensity and lightning probability?, *Mon. Weather Rev.*, *122*, 1751–1759, 1994.

---

S. Sherwood, Yale University, New Haven, CT 06520 (ssherwood@alum.mit.edu)

Received \_\_\_\_\_

---

This manuscript was prepared with AGU’s L<sup>A</sup>T<sub>E</sub>X macros v4, with the extension package ‘AGU++’ by P. W. Daly, version 1.5e from 1997/11/18.

## Figure Captions

**Figure 1.**  $Z_{11}$  from GOES-8 vs.  $Z_{\text{lid}}(1)$  from the CPL lidar.

**Figure 2.** CPL volumetric extinction coefficient averaged as a function of distance above  $Z_{\text{lid}}(1)$ , for several  $T_{11}$  ranges. Typical height of GOES  $Z_{11}$  also indicated.

**Figure 3.**  $Z_{11}$  from MODIS vs.  $Z_{\text{ster}}$  from MISR, for three Florida overpasses of Terra during CRYSTAL-FACE.

**Figure 4.** Height histograms for  $Z_{\text{ster}}$ , and for  $Z_{11}$  using three  $T(Z)$  models (“MOD-1,2,3” refers respectively to the “adiabatic-1”, “adiabatic-2” and “semiadiabatic” models described in text).

## Figures

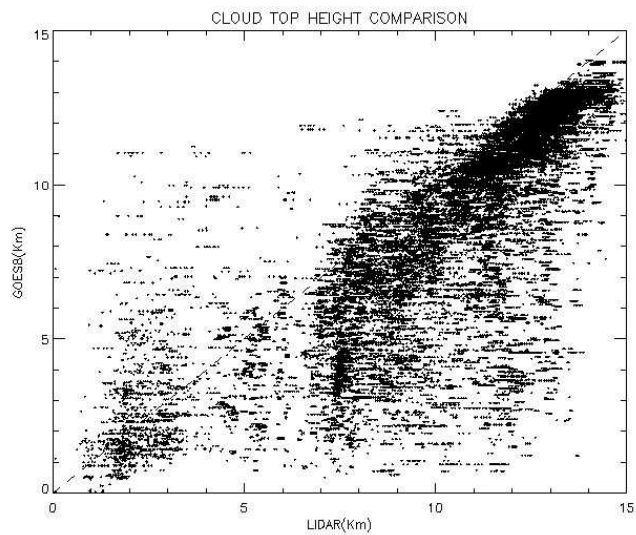


**Figure 1.**  $Z_{11}$  from GOES-8 vs.  $Z_{lid}(1)$  from the CPL lidar.

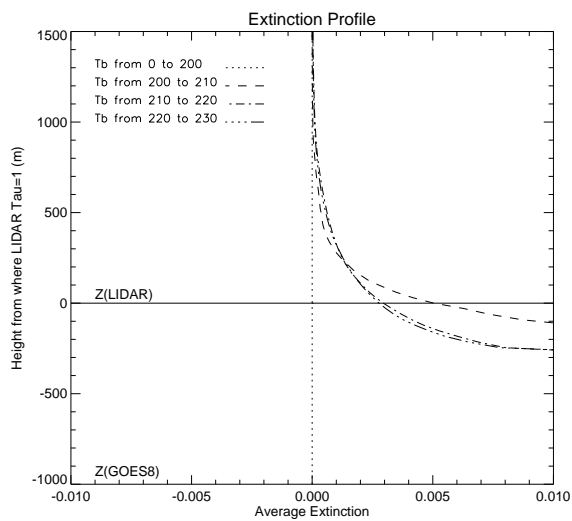


**Figure 2.** CPL volumetric extinction coefficient averaged as a function of distance above  $Z_{lid}(1)$ , for several  $T_{11}$  ranges. Typical height of GOES  $Z_{11}$  also indicated.

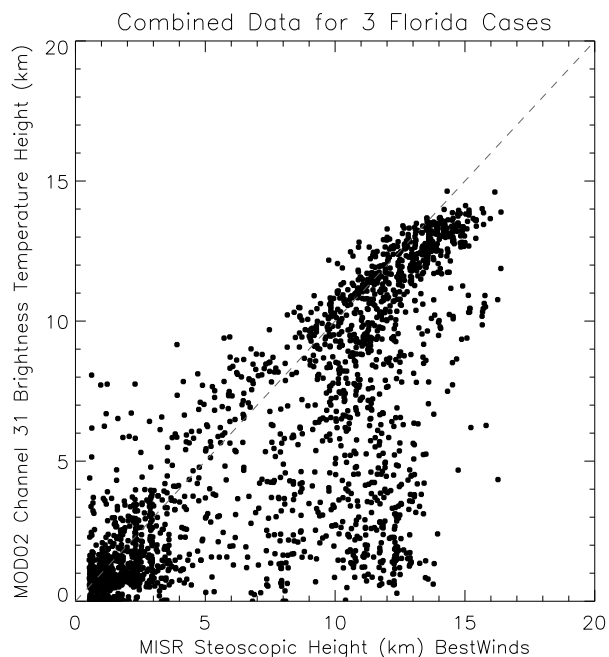


**Figure 3.**  $Z_{11}$  from MODIS vs.  $Z_{ster}$  from MISR, for three Florida overpasses of Terra during CRYSTAL-FACE.

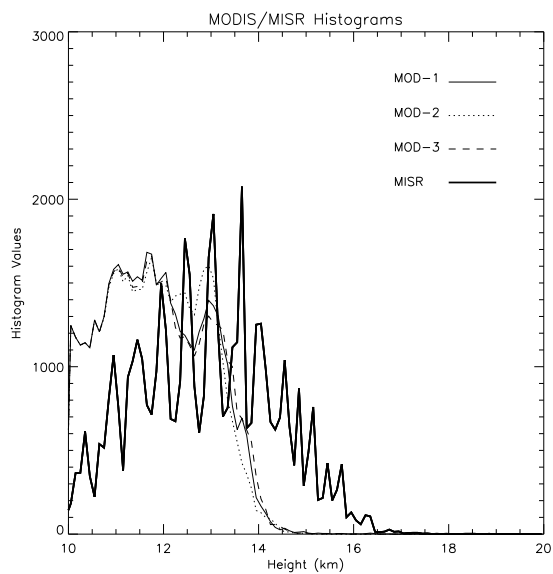


**Figure 4.** Height histograms for  $Z_{ster}$ , and for  $Z_{11}$  using three  $T(Z)$  models (“MOD-1,2,3” refers respectively to the “adiabatic-1”; “adiabatic-2” and “semiadiabatic” models described in text).